

# Tunable Mechanical, Electrical, and Thermal Properties of Polymer Nanocomposites through GMA Bridging at Interface

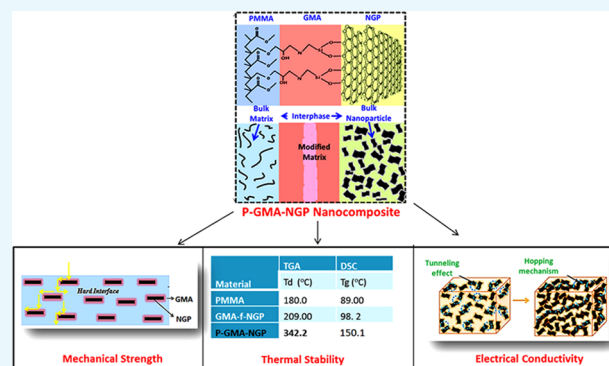
Payal Mazumdar,<sup>†</sup> Sreekumar Chockalingam,<sup>‡</sup> Sunita Rattan,<sup>\*,†</sup> and Bipin Kumar Gupta<sup>\*,†</sup>

<sup>†</sup>Amity Institute of Applied Sciences, Amity University, Sector-125, Noida 201313, UP, India

<sup>‡</sup>CSIR-National Physical Laboratory, New Delhi 110012, India

## Supporting Information

**ABSTRACT:** Polymer nanocomposites (PNCs) have become an exciting field of current research and have attracted a huge interest among both academia and industry during the last few decades. However, the multifunctional single-nanocomposite film exhibiting the combination of desired structure and properties still remains a big challenge. Herein, we report a novel strategy to address these problems by using versatile polymer glycidyl methacrylate (GMA) as a bridging medium between the filler and the polymer matrix, resulting in high density of interfaces as well as strong interactions, which lead to generation of tunable thermal, mechanical, and electrical properties in the materials. The nanocomposites prepared by GMA bridging exhibit the remarkable combination of thermal ( $T_d = 342.2$  °C,  $T_g = 150.1$  °C), mechanical ( $E = 7.6$  Gpa and  $H = 0.45$  Gpa) and electrical ( $\sigma = 3.15 \times 10^{-5}$  S/cm) properties. Hence, the conjugation approaches related to GMA bridging facilitate a new paradigm for producing multifunctional polymer nanocomposites having a unique combination of multifunctional properties, which can be potentially used in next-generation polymer-based advanced functional devices.



## INTRODUCTION

Since the evolution of nanographite platelets (NGPs) composed of few graphene layers through exfoliation of graphite, it has been proven to be a perfect two-dimensional (2D) crystal exhibiting unparalleled properties in a number of fields. Nanographite platelets (NGPs), with a platelet thickness less than 0.34–100 nm, are widely used because of their high surface area, light weight, flexibility, high thermal stability, excellent mechanical strength, remarkable electrical conductivity, low cost, and ease of synthesis as compared to single-layer graphene while retaining the desirable properties.<sup>1,2</sup> The NGPs provide a realistic and useful alternative to CNT, CNFs, and possible graphene in a wide range of applications and natural abundance of their precursor graphite.<sup>3,4</sup> In spite of their irregular shape, NGPs are preferred over other conventional fillers because they give more freedom to the polymer nanocomposite (PNC) material due to their better structural and functional properties and broad range of applications.

There are numerous studies in the progress of polymer nanocomposites; unfortunately, the need of a multifunctional single composite film exhibiting altogether the impressive properties (structural, thermal, mechanical, and electrical) remains a challenge. Haddon et al. reported the synthesis of polymer nanocomposite by dispersing nanographite platelets into the epoxy matrixes for excellent thermal conductivity at low filler loading.<sup>5</sup> Moreover, Veca et al. reported the flexible nanocomposite films synthesized by epoxy and few layer

nanographite platelets for delivering a high conductivity.<sup>6</sup> Chen et al. paid major attention to the study of the strong interfacial interaction between multiwall carbon nanotube and polyetherimide achieved through poly(9,9-dioctylfluorenyl-2,7-diyl) coatings to provide remarkable mechanical and electrical conductivity in the composite film.<sup>7</sup> Among these recent reports, Zhang et al. proposed a versatile approach to synthesize a graphene/poly(methyl methacrylate) (PMMA) composite with remarkable mechanical behavior by tuning the interfacial region.<sup>8</sup> Recently, Wang et al. studied the aspects on the improvement of the thermal transport across the interface between graphene and epoxy nanocomposites by using molecular dynamics (MD) simulations.<sup>9</sup> Despite all these studies, (i) uniform distribution and (ii) strong interfacial interaction between the filler and the matrix, which defines the properties of the entire composite system, remains an open question.<sup>10–13</sup>

It is generally accepted that the change in interface plays a significant role in affecting the structure/organization, dynamics, and properties of the polymer nanocomposite that actually define and integrate new character in the material. The alterations in chemistry and mobility in interface region have a drastic impact on the bulk properties of the composite. The

Received: February 1, 2018

Accepted: March 21, 2018

Published: April 2, 2018

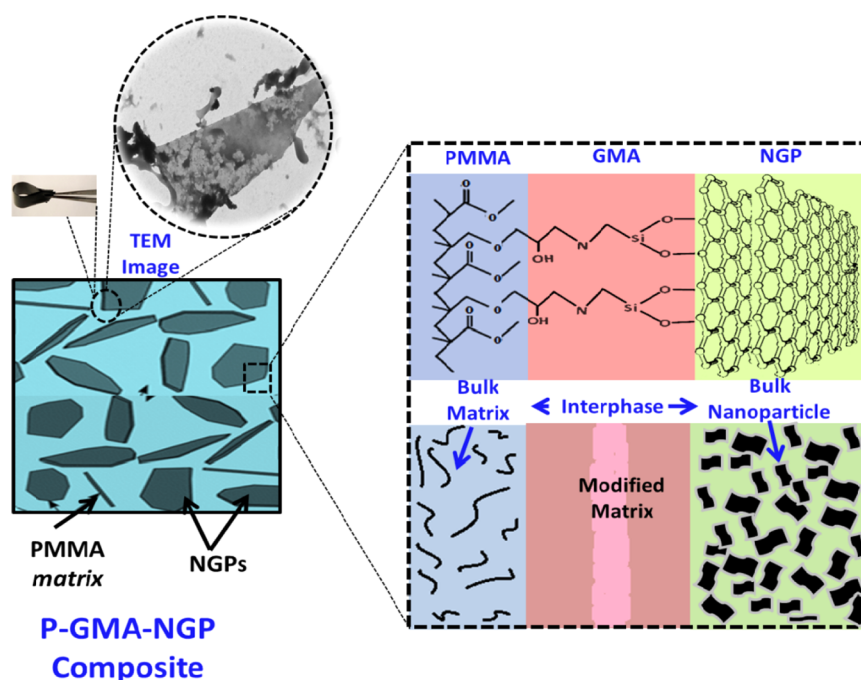


**Figure 1.** Schematic representation of GMA interphases between PMMA matrix and NGP filler.

effort to examine the interfacial properties and then clarify the impact of interfacial bonding types (e.g., van der Waals forces, H-bonds, covalent bonds, coordinate bonds) on the interfacial behaviors are critical and indispensable for polymer nanocomposite materials.<sup>14</sup> To the best of our knowledge, few theoretical studies performed to analyze the interfacial properties of the composites through atomistic modeling were below expectation.<sup>15</sup> Thus, the properties of the polymer nanocomposite can be fully realized if its interfacial region is extended through the progression of suitable linkages by using appropriate processing route. Thus, the judicious selection of processing route diminishes the interfacial tension and suppresses the agglomeration between the filler and the matrix.<sup>16–21</sup> In last few years, we have attempted novel processes such as melt mixing, swift heavy ion irradiation,<sup>22</sup> and click chemistry<sup>23,24</sup> for providing a high density of the interfaces and strong covalent linkages between the filler and the matrix.

In the present investigations, polymer nanocomposites were designed through a novel strategy by using glycidyl methacrylate bridge for not only developing tailor-made properties but also controlling the chemistry, which totally differs from those of bulk matrix. The glycidyl methacrylate (GMA) not only alters the enthalpic and entropic interfacial interaction and the proclivity of aggregation but also reduces the interfacial tension, interfacial failure, and dispersed-phase coalescence between the NGPs and PMMA matrix. The legitimate selection of GMA as reactive compatibilizer containing both acrylic and epoxy groups provides an opportunity in designing new material with simultaneous improvement in thermal, mechanical, and electrical properties, which make it light weight, low-cost, flexible, and durable material. Polymer nanocomposites were prepared, compared, and fully characterized using Fourier transform infrared (FTIR), X-ray diffraction (XRD), thermogravimetric analysis (TGA), differential scanning calorimetry (DSC), scanning electron microscopy (SEM), and transmission electron

microscopy (TEM). More than the conventional studies, the X-ray photoelectron spectroscopy (XPS) is also utilized to elucidate the polymer/filler interaction. Conductivity studies, as well as nanomechanical and thermal properties of P-GMA-NGP composites, are also discussed in detail.

## ■ RESULT AND DISCUSSION

It is accepted by the researcher that the interaction between the filler and polymer matrix at the interface plays a crucial role in enhancing the structural properties of the entire composite. By understanding the characteristics of interface region, it is possible to predict as well as design polymer nanocomposites with preferred properties and performance as shown in [Figure 1](#). To enhance the overall performance of polymer nanocomposite, properties of the interphase should be tailored by improving the intrinsic properties of both the matrix and the nanofiller. Moreover, it is considered that the dominant failure mode in filler-reinforced polymers is the interphase related to debonding between matrix and filler, its detection and even healing are particularly preferred.

A robust and flexible P-GMA-NGP film with a firm luster is attained by GMA functionalization of NGP surfaces (GMA-f-NGPs). Moreover, these films are soluble in a wide variety of organic solvents ( $\text{CHCl}_3$ , benzene, toluene, acetone, tetrahydrofuran (THF), and dimethylformamide), provided that the solvent effectively solvates the PMMA polymer ([Figure S1a,b](#)). Conversely, a solvent that does not dissolve PMMA is also incapable of dissolving its composites, as polymer plays the key role to define the solubility properties of the composite material.<sup>25,26</sup> All of the hybrid solutions of P-GMA-NGP could stand high-power sonication and remain homogeneous and stable with no discernible particulate or precipitate of black agglomeration for almost one month, indicating the NGPs are bonded to the solvated polymer.

[Figure 2](#) represents the FTIR spectrum of composite before and after the surface treatment of NGPs. Pristine NGP shows that typical characteristic peaks at 3430, 1115, and 1069  $\text{cm}^{-1}$

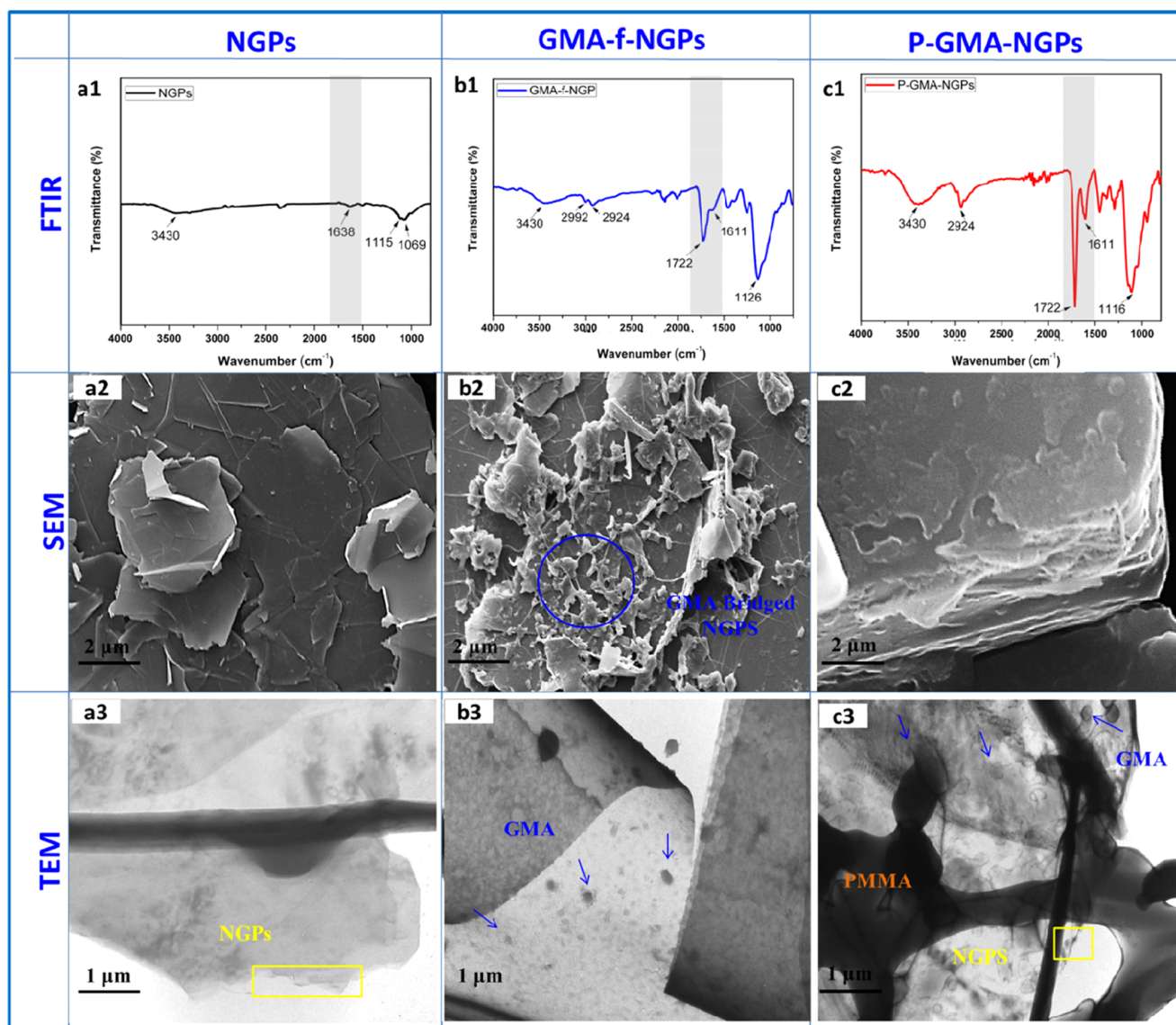


**Figure 2.** FTIR spectra of (a1) NGPs, (b1) GMA-f-NGPs, and (c1) P-GMA-NGPs. SEM and TEM morphology of (a2, a3) NGPs, (b2, b3) GMA-f-NGPs, and (c2, c3) P-GMA-NGPs.

arises from hydroxyl groups, C=C, and C–O epoxide groups, respectively. Upon GMA functionalization, the reactive epoxy groups of GMA attached to a polymer backbone offers numerous possibilities for modification of NGP surface by nucleophilic ring opening of epoxide. The new peaks at 1722 and 1611 cm<sup>-1</sup> depicting –C=O and –C=C stretching vibrations were observed, which shows the successful covalent bonding between NGPs and GMA via the ring-opening reaction.<sup>27</sup> However, the distinct peaks are not present in the precursor NGPs. After in situ polymerization, the band intensity of P-GMA-NGPs composite shows a great enhancement, which is attributed to GMA-f-NGPs overlapped with the characteristic peaks of PMMA indicating the improved adhesive bonding via interfacial cross-linking of the GMA chains with the PMMA matrix. Moreover, band ranging from 1150 to 1250 cm<sup>-1</sup> is due to the presence of distinct characteristic absorption of pure PMMA polymer.<sup>28</sup> The morphological studies of the composites were analyzed by using scanning electron microscopy (SEM) and transmission electron microscopy (TEM). Figure 2a2 shows the flat wrinkled surface with a

carpet-like morphology and no evident stack layers depicting the presence of nanoplatelets. After GMA functionalization, one can clearly observe the GMA embedded on the sheets of nanographite in Figure 2b2. A well-dispersed small darker spots of GMA with no significant agglomeration exhibits the success of GMA functionalization on the surface of NGPs. Moreover, the functionalization of NGPs by GMA led to a substantial increase in dispersion. Upon in situ polymerization, the P-GMA-NGP composite depicts the homogeneous dispersion of NGPs in PMMA matrix without any aggregation due to the empowered compatibility between the filler and polymer matrix through GMA bridging. Overall, it is evident from Figures 2c3 and S2 that all of the three components have achieved a uniform distribution, which is mainly due to the bridging of GMA particles between the NGP and PMMA matrix. This interconnected morphology leads to a nanoscale surface roughness, which is likely to produce an enhanced mechanical interlocking and adhesion between the filler and the matrix.

XRD is an effective technique to estimate the interlayer changes of graphite-related samples and its dispersion in the

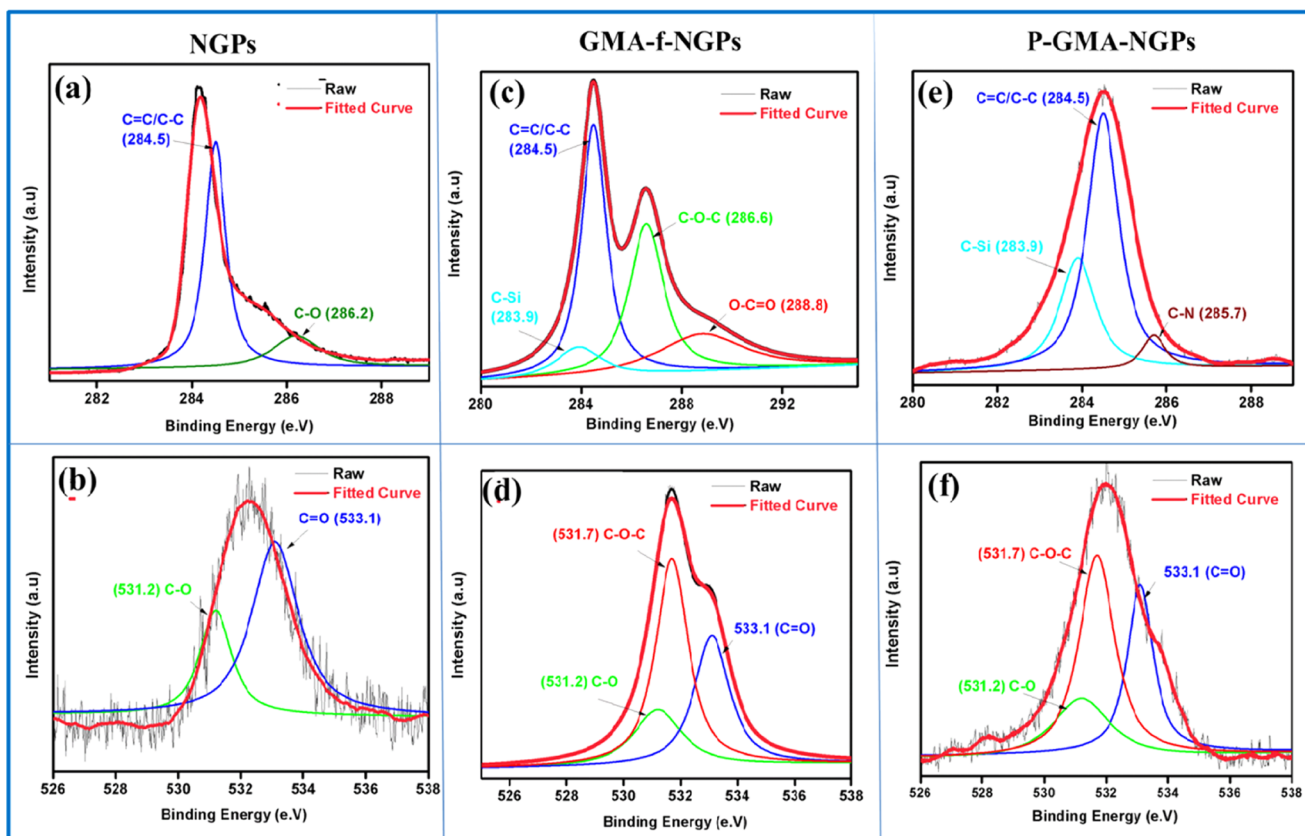


**Figure 3.** XPS spectra and deconvolution results for C 1s and O 1s for (a, b) NGPs, (c, d) GMA-f-NGPs, and (e, f) P-GMA-NGPs.

polymer matrix. As shown in Figure S3, the XRD patterns of NGP exhibit a sharp (002) graphite characteristic peak at  $2\theta = 26.7^\circ$  with 0.34 nm interlayer spacing.<sup>29</sup> However, after functionalization of NGPs with GMA chains (GMA-f-NGPs), the sharp peak of NGP diminishes, suggesting the disorder and loss of structural regularity of the nanographite layers. Matsumoto et al.<sup>30</sup> reported the similar decrease in the intensity of (002) diffraction peak, which was attributed to the exfoliation of graphite into isolated graphene sheets. Further, the P-GMA-NGP composite depicts a significant decrease in the peak intensity, indicating the delamination of the NGPs on the way to the formation of few-layered graphene platelets.<sup>31,32</sup> The subsequent interlayer polymerization makes PMMA linkages graft covalently onto the surface of NGPs, which results in exfoliation into or few-layered platelets.

XPS is used to study the quantitative and qualitative chemical analysis of functional groups grafted on the surface of NGPs. Figure 3 shows the deconvoluted XPS spectra for the C 1s and O 1s orbitals, and the binding energies of the grafted functional groups. The XPS spectrum of NGP, GMA-f-NGP, and P-GMA-NGP composite depicts the raw data and the deconvolution results resolved by the Gaussian-Lorentzian data fit. The intense C 1s peak of NGPs in Figure 3a with graphitic structures C=C/C-C (85.4%) and C-O (14.5%) at binding energy 284.5 and 286.2 eV, respectively, depicts the presence of carbon functional groups. Additionally, the deconvoluted O 1s region of NGPs in Figure 3b exhibits two binding energies located at 533.1 and 531.2 eV, which are assigned to C=O and C-O, respectively. However, after GMA functionalization, the disappearance of C-O at 286.2 eV (14.5%) along with the appearance of C-O-C at 286.6 eV (38.8%) epoxide rings confirms the successful modification of NGP surfaces by GMA

compatibilizer, which effectively binds itself across the interface promoting a homogeneous distribution of the NGPs within the PMMA matrix (Figure 3c).<sup>33,34</sup> The GMA introduces large entropic components, which favors the uniform dispersion of NGP fillers and PMMA matrix. Additionally, the analysis of the C 1s orbital energies also provides evidence of a C-Si bond at 283.9 eV, which is due to the pretreatment of NGPs by silane coupling agent. Compared to GMA-f-NGPs, the intensity of C=C/C-C at 284.4 eV for P-GMA-NGP composite increases from 37.2 to 66% due to the presence of PMMA chains in the composite system (Figure 3e). Additionally, the O 1s peak representing C=O at 533.1 eV for P-GMA-NGP composite (38.9%) becomes much stronger than that for GMA-f-NGP (32.5%), suggesting an effective in situ polymerization reaction (Figure 3f).<sup>35-37</sup> The survey scan XPS spectra of NGPs, GMA-f-NGP, and P-GMA-NGPs considerably from binding energy 0–1000 eV which relates to the O 1s, N 1s and Si 2p atoms are depicted in Figure S4.

The thermal properties of the P-GMA-NGP composite film prepared by GMA bridging method were compared with those of P-NGP/S composite prepared by conventional solution-blending method. The thermogravimetric analysis (TGA) and differential scanning calorimetry (DSC) techniques were used to determine the thermal stability of the composite as shown in Figure 4. The TGA thermograms of PMMA and polymer nanocomposites were obtained under a nitrogen atmosphere. Figure 4a depicts the thermal decomposition temperature of PMMA, GMA-f-NGPs, P-NGP/S, and P-GMA-NGP. Thermolysis of GMA-f-NGP and consequently its main mass loss happen at around 209 °C, which was continued rapidly and then degraded at 400 °C. The enhancement in the thermal decomposition temperature ( $T_d$ ) indicates the presence of

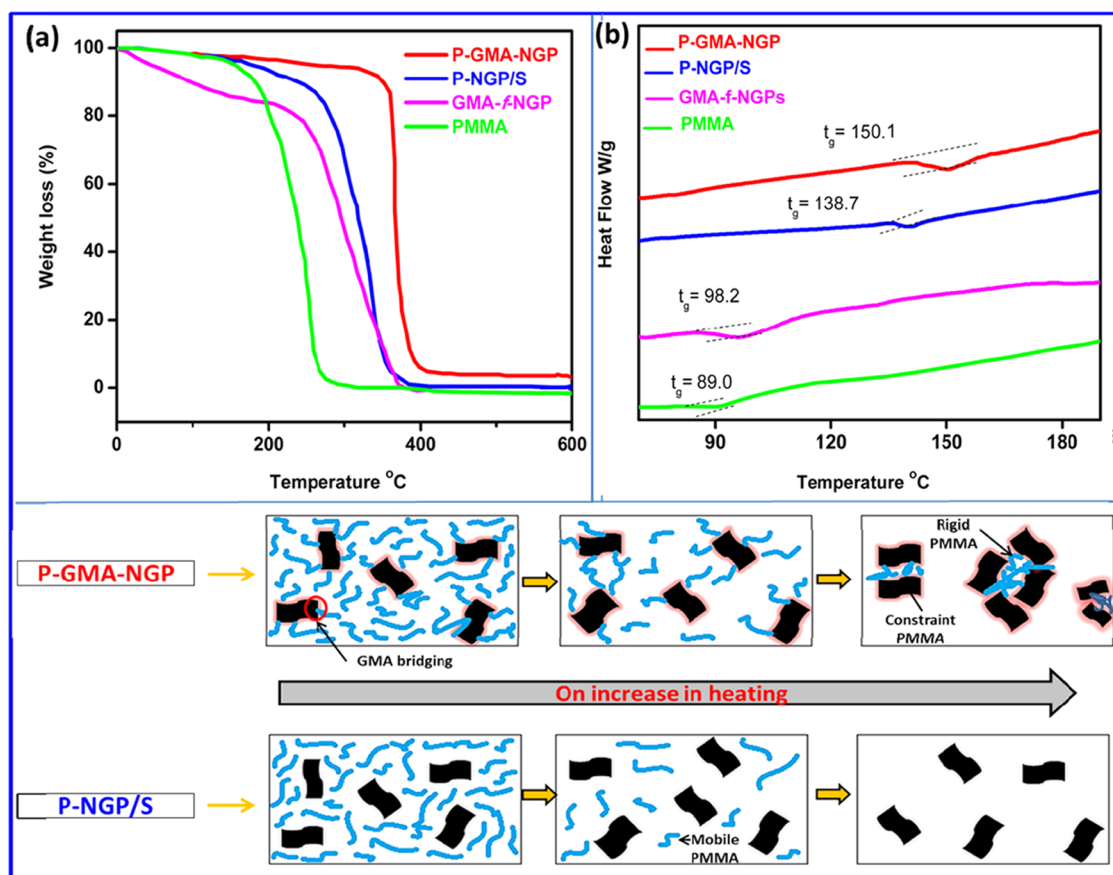


**Figure 4.** (a) TGA and (b) DSC thermograms of PMMA, GMA-f-NGPs, P-NGP/S, and P-GMA-NGP.

GMA functionalized chains on the surface of NGPs by free-radical addition, which increases the thermal stability. After polymerization, a substantial increase of approximately 80 °C in the thermal decomposition temperature of P-GMA-NGP ( $T_d = 342$  °C) was observed than in that of P-NGP/S synthesized by the solution-mixing method (245 °C). Compared to P-NGP/S synthesized by the solution-mixing method, a remarkable increase in the thermal stability of P-GMA-NGP composite was observed due to the strong interfacial interaction between the polymer filler through the bridging of GMA chains, which hinders the decomposition.<sup>38,39</sup> Moreover, a higher residue of P-GMA-NGP at 600 °C can be attributed to earlier functionalization of NGPs, which plays an important role during the degradation of nanocomposite and leads to the formation of a thermally stable product and contributes to the residue formation in the end.

The glass transition temperatures of PMMA and its composites were evaluated by using DSC as depicted in Figure 4b. For pure PMMA and GMA-f-NGPs, the values of  $T_g = 89$  and 98.2 °C were recorded, respectively. There is an increase in the glass transition temperature of the nanocomposites as compared to pure PMMA, which is tentatively attributed to the confinement effect of the polymeric chains inside the NGP galleries that restricts the movement of the polymeric chains. Moreover, a prominent increase in the  $T_g$  of P-GMA-NGP ( $T_g = 150.1$  °C) synthesized through GMA bridging method as compared to P-NGP/S composite ( $T_g = 138.7$  °C) prepared by the solution-blending method was observed. The elevation in the  $T_g$  value of P-GMA-NGP is attributed to the uniform dispersion of NGPs through GMA functionalization and strong

covalent interaction between GMA and NGPs at the surface.<sup>40,41</sup>

The molecular weight of the polymer nanocomposites was studied by using the gel permeation chromatography (GPC). The weight average molecular weight ( $M_w$ ) and the number average molecular weight ( $M_n$ ) decrease steadily with the incorporation of GMA-f-NGPs within the PMMA matrix. Although the  $M_w$  decreases significantly from 234 279 g mol<sup>-1</sup> for PMMA to 101 000 g mol<sup>-1</sup> for P-GMA-NGPs, the  $T_g$  value still indicates an improvement (Table 1). This observation

**Table 1.** Relationship of the Composite of Polymer Nanocomposites Material with Molecular Weight ( $M_w$ ,  $M_n$ ) Polydispersity Index (PDI),  $T_d$ , and  $T_g$  Measured from GPC, TGA, and DSC

material	GPC measurement			TGA	DSC
	$M_w$ (g mol <sup>-1</sup> )	$M_n$ (g mol <sup>-1</sup> )	PDI	$T_d$ (°C)	$T_g$ (°C)
PMMA	234 279	149 335	1.56	180.00	89.0
GMA-f-NGP	101 000	50 081	2.00	209.00	98.2
P-GMA-NGP	87 547	31 223	2.80	342.2	150.1
P-NGP/S	218 090	140 000	1.55	245.00	138.7

indicates the presence of a strong interfacial interaction between GMA-f-NGPs and the PMMA matrix, which constrains the association of the polymeric chains during heating. Therefore, this study shows that the functionalized GMA chains on the NGP surface limits the mobility of the composite, which provides a positive assistance to the glass

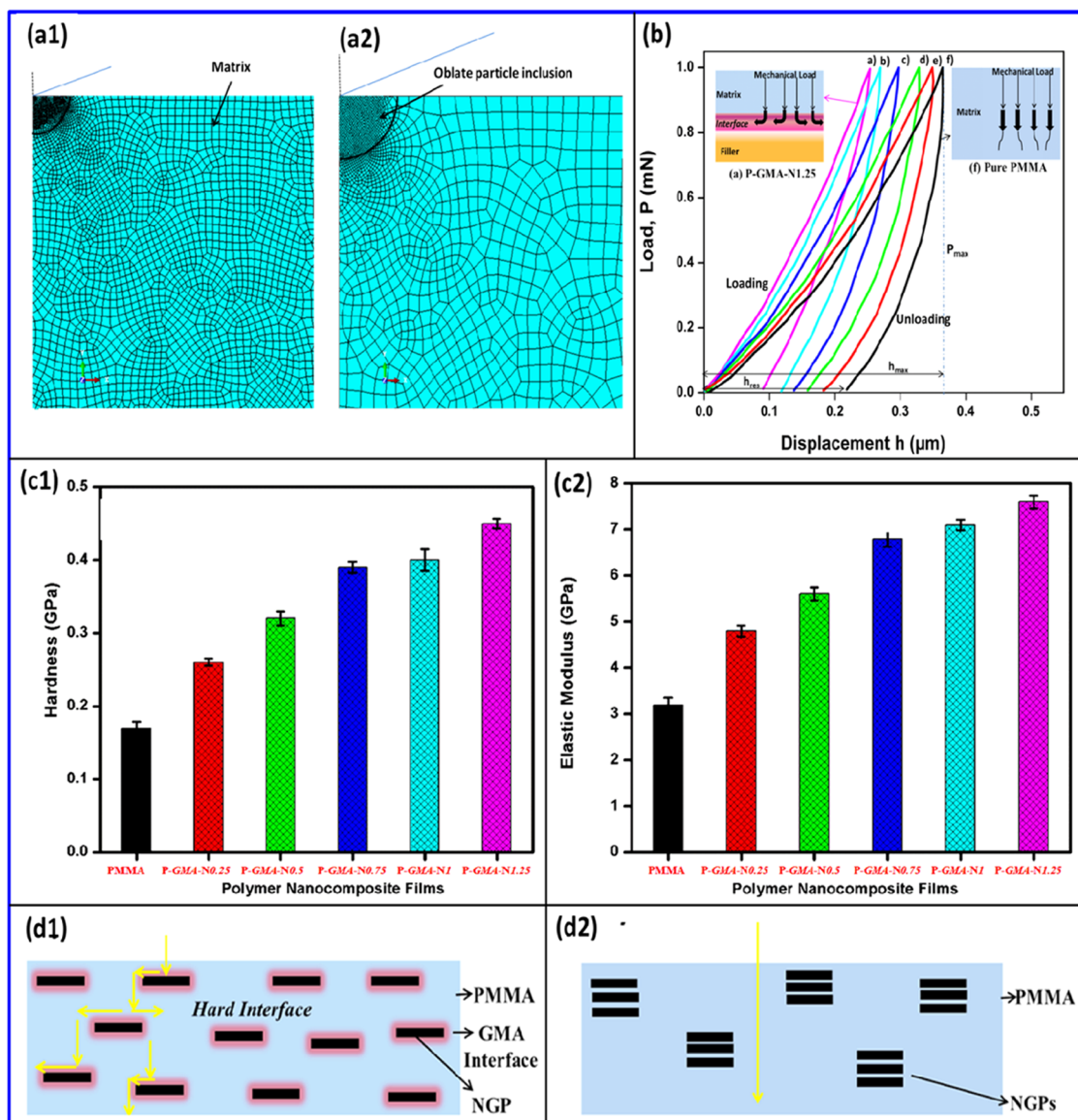


**Figure 5.** (a1–a2) Details of the finite element mesh of indentation of embedded oblate NGP particles in the PMMA matrix. (b) Load versus displacement curves of (i) P-GMA-N1.25 (ii) P-GMA-N1 (iii) P-GMA-N0.75 (iv) P-GMA-N0.5 (v) P-GMA-N0.25 and (vi) PMMA films at 1mN load. (c1) Hardness and (c2) Elastic Modulus values of P-GMA-NGPs by GMA bridging method. Schematic depicting penetration of Berkovich indenter on polymer nanocomposite films prepared by (d1) GMA bridging method and (d2) solution blending method.

temperature to compensate for the loss of the  $T_g$  from the decrease in molecular weight prepared by GMA bridging.<sup>42</sup>

The mechanical properties of the polymer nanocomposite are closely related to electrical and thermal properties to determine their performance for various structural applications. To accurately characterize the behavior of the material at local sites, the mechanical properties are investigated by using a nanoindentation technique. Nanoindentation is a powerful and advanced way for measuring the mechanical properties of polymer nanocomposites.<sup>43</sup> The aim of the nanoindentation experiment is to determine various parameters related to the mechanical behavior of the composite to study the structure, bond strengths, flexibility, durability, and strength of the local surface of the polymer nanocomposite films.<sup>44</sup> Moreover, the nanoindentation technique also represents to study the distribution of filler in the polymer matrix by mapping of the surface at various micrometers by the indenter. The accuracy of the measurements greatly affects the reliability of the

subsequent data analysis. The nanoindentation testing followed by analytical modeling was studied for P-GMA-NGP composite system. These polymer nanocomposites based on partially exfoliated and intercalated functionalized NGP nanofillers are embedded within the PMMA matrix for evaluation in the nanoscale range. The nanofillers are always considered to be spherical, cylindrical, or disk shaped. In the present investigation, the intercalated NGP fillers within the polymer galleries are considered as equivalent oblate nanofillers for modeling. Finite element (FE) analysis was conducted by using oblate NGP fillers with a radius  $>100$  nm. The Poisson ratio and thickness of composite were assumed to be 0.3 and  $0.5 \mu\text{m}$ , respectively. It was also assumed that NGP fillers were uniformly distributed such that the indentation stress field will not be affected by the neighboring particles. As the volume fraction of the particle was low (0.25 wt %), the filler distribution inside the PMMA polymer matrix at the nanometer scale was treated as anisotropic distribution. A typical conical

tip Berkovich indenter with the semi-included angle of  $70.3^\circ$  and a tip radius of 40 nm was used in the study.<sup>45</sup> Due to the symmetric nature of the indenter and the composite specimen, a 2D axis symmetric finite element model was developed using ABAQUS for simulation.<sup>46,47</sup> Figure 5a1 shows the finite element (FE) mesh of the P-GMA-NGP nanocomposite system. Further, the zoomed image (Figure 5a2) depicts a very fine mesh in the contact zone beneath the indenter tip to ensure the accuracy of the numerical results. A total of 10 350 elements were used to model the nanoparticle and the matrix. The output indentation force versus the indentation depth curve was then used to predict the hardness and elastic modulus of the particle by following the Oliver–Pharr method, which was conducted by a nanoindentation instrument through a physical test. For this purpose, the Oliver–Pharr method is first briefly discussed.

Nowadays, Oliver–Pharr model<sup>48</sup> is extensively used for the analysis of load–displacement curve by the incorporation of the procedure into the software. The elastic–plastic materials show most successful and appropriate calibration of the machine compliance, tip area function, and thermal drift. The hardness ( $H$ ) and the elastic modulus ( $E$ ) values were attained from the simulated data of polymer nanocomposite films obtained from the load–displacement curves by the Oliver–Pharr method. The loading part of the curve was the combination of elastic and plastic deformation, and the unloading curve was dominated by elastic deformation. The mechanical properties of the surfaces are significant for the comprehension behavior of matrix and the incorporated filler material. A characteristic nanoindentation adhesion test is comprised of pressing the tip into the patterned sample, followed by unloading it at a constant rate, and finally obtaining a distinctive pull-off force representing the adhering surfaces. All the fitting parameters and their respective formulas obtained by loading–unloading curves have been illustrated in our previous study.<sup>22</sup> The as-prepared P-GMA-NGP polymer nanocomposite films were further investigated by load–displacement curve. The nanoindentation method was adopted to analyze the load–depth data by depth sensing of the films using a sharp Berkovich indenter. In this procedure, nanoindentation hardness ( $H$ ), elastic modulus ( $E$ ), brittleness index (or  $H/E$  ratio), wear resistance, and recovery index of free-standing polymer nanocomposite films without any substrate was proposed. In Figure 5b, the variation in the load–displacement curves of polymer nanocomposites were denoted as P-GMA-NGP with increasing NGP loading from 0.25 to 1.25 wt % named as P-GMA-N0.25, P-GMA-N0.5, P-GMA-N0.75, P-GMA-N1, and P-GMA-N1.25. The graph represents the decrease in the value of depth of the residual impression ( $h_{res}$ ) with increase in the NGP wt %. It is evident from the figure that for 1 mN load, the load–displacement curves appear to be smooth and no pop-in and no detectable crack was observed during the whole loading–unloading cycle.<sup>49</sup> It is important to point out that the nanoindentation experiment was performed on at least 10 samples for each loading fraction and no significant changes were found, demonstrating the uniform distribution of the filler in the matrix.

The hardness ( $H$ ) and elastic modulus ( $E$ ) values for polymer nanocomposite films prepared by GMA Bridging were extensively studied by using the load–displacement curve. Conventional nanoindentation hardness refers to the mean contact pressure; this hardness, which is the contact hardness, is actually dependent on the geometry of the indenter.<sup>50,51</sup> Figure

5c1 depicts the hardness profile of P-GMA-NGP as a function of NGP wt %. It is observed that the value of  $H$  for pure PMMA is 0.17 GPa, which is increased up to 0.26 GPa with only 0.25% of modified NGPs and then to 0.45 GPa for 1.25 wt % of filler loadings. During the indentation process, the indenter is in contact with modified NGP particles embedded homogeneously in the PMMA matrix, which exhibits a substantial increase in the hardness of the complete composite system. Thus, the uniform distribution obtained by the GMA bridging method is one of the most important factors that support the increase in the hardness of the P-GMA-NGP composites at increasing loadings. Similarly, the values of the elastic modulus increased following the same trend, which mainly depends on the slope of harmonic interatomic potential. It is evidently seen in Figure 5c2 that at a small weight fraction of 1.25% filler loadings, the effective increase in the elastic modulus reaches to 7.6 GPa, which is a significant increase of 4.4 GPa compared to that of pure PMMA matrix. Till date, there is no report in literature depicting such a remarkable increase in elastic modulus and hardness for polymer nanocomposite films prepared by various methods (Table S1). Fundamentally, in the case of P-GMA-NGP composites, the mechanical load applied to the polymer matrices was transferred to the reinforced nanofillers via interphase, and such a behavior depends on the structural and mechanical properties of the interfacial bond between the polymer and filler as shown in Figure 5d1. A strong bond means an efficient load transfer; thus, it has a positive effect on the mechanical properties of nanocomposites. However, for P-NGP/S prepared by the typical solution-blending method, the presence of a weak bond indicates a lack of load transfer, which may cause crack initiation/propagation along the interphase of the nanocomposites (Figure 5d2). All of these results reflect the superior mechanical properties of P-GMA-NGP compared to P-NGP/S composites due to the strong covalent bonding between the NGP and PMMA achieved through GMA linkages at the interface.<sup>52,53</sup> The error bars in the graphs represent the standard deviation of the calculated values of the hardness and elastic modulus.

To further investigate the influence of processing techniques on the preparation of polymer nanocomposites, fractured SEM images and optical microscopy images are studied in detail. Figure S5a1,b1 depicts the fractured SEM images of P-GMA-NGP and P-NGP/S nanocomposites. As depicted in the morphology, the P-GMA-NGPs shows a strong interaction in comparison with P-NGP/S nanocomposites, which is due to the versatile GMA, which binds NGP through functionalization on one end and covalently bonded with the PMMA matrix on the other end. Thus, the GMA bridging increases the volume of the interaction and bonding between the polymer and filler. Moreover, the nanosize layers are observed to be distributed evenly in the fractured surface of P-GMA-NGPs, which was attributed to the high specific areas of NGPs along with the uniform dispersion of the filler within the polymer matrix. However, for P-NGP/S, the clusters of agglomerated PMMA and microvoids are clearly visible on the fracture surface. Moreover, the simplest test to determine whether the NGPs are dispersed homogeneously in the polymer matrix is through an optical microscope. The P-GMA-NGP shows the uniform distribution of the modified NGPs within the PMMA matrix in Figure S5a2; however, for P-NGP/S, Figure S5b2 clearly depicts an uneven distribution of black spots, which is due to the irregular distribution of the NGPs into the host matrix. For

Table 2. Representation of Nanoindentation Values of P-GMA-NGPs and P-NGP/S as a Function of NGP wt %

composition	displacement ( $h$ , $\mu\text{m}$ )	$H$ (GPa)	$E$ (GPa)	$H/E$	ER%	$h_{\text{res}}/h_{\text{max}}$	$U_r$
PMMA	0.220	0.17	3.2	0.0531	23.2	0.597	$9.97 \times 10^{-9}$
P-GMA-N0.25	0.179	0.26	4.8	0.0541	49.7	0.502	$8.07 \times 10^{-9}$
P-GMA-N0.5	0.158	0.32	5.6	0.0571	52.4	0.475	$7.27 \times 10^{-9}$
P-GMA-N0.75	0.141	0.39	6.8	0.0573	52.8	0.471	$6.58 \times 10^{-9}$
P-GMA-N1	0.123	0.40	7.1	0.0563	55.2	0.447	$6.50 \times 10^{-9}$
P-GMA-N1.25	0.101	0.45	7.6	0.0592	60.3	0.396	$6.13 \times 10^{-9}$
P-N0.25/S	0.215	0.18	3.4	0.0529	25.7	0.541	$9.69 \times 10^{-9}$
P-N0.5/S	0.205	0.18	3.4	0.0529	24.1	0.538	$9.68 \times 10^{-9}$
P-N0.75/S	0.189	0.18	3.9	0.0461	27.7	0.456	$9.65 \times 10^{-9}$
P-N1/S	0.181	0.19	4.0	0.0475	32.5	0.408	$9.45 \times 10^{-9}$
P-N1.25/S	0.177	0.24	4.9	0.0489	39.9	0.401	$8.40 \times 10^{-9}$

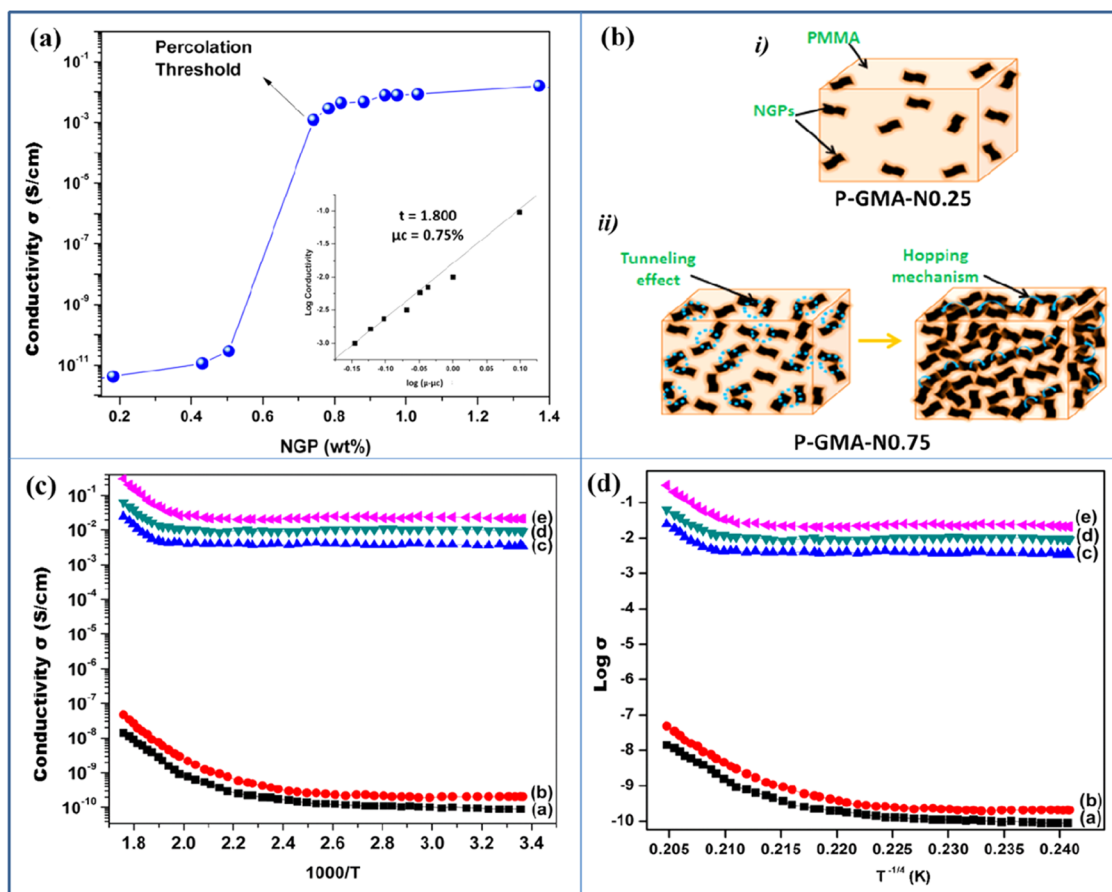


**Figure 6.** (a) Plot of electrical conductivity of PNCs vs NGP filler content. The inset is a double logarithmic plot of volume electrical conductivity vs  $(\mu - \mu_c)$  with the fitted parameter of  $t = 1.80$ ,  $\mu_c = 0.75$  wt %. (b) Schematic depicting the tunneling effect of increasing conductivity. (c) Conductivity vs the inverse of absolute temperature for P-GMA-NGP composite films as a function of NGP wt %. (d)  $\text{Log } \sigma$  vs  $T^{-1/4}$  curves for P-GMA-NGP nanocomposite films.

further evaluation, the SEM micrograph of polymer nanocomposites prepared by GMA bridging method was compared with the solution-blending method. Figure S5a3 depicts a well-resolved feature in which NGPs are homogeneously dispersed within the PMMA matrix; in contrast, P-NGP/S exhibits the agglomeration, which may promote macroscopic defects that can lead to the breakdown or failure of mechanical strength (Figure S5b3).

Besides hardness and elastic modulus, wear resistance<sup>54</sup> was also found to be an important property for protective hard coatings. The indirect estimation of wear resistance using plastic resistance parameter ( $H/E$ ) was attributed as an

important parameter to explain the elastic–plastic behavior of the polymer nanocomposite films. The domain of the validity of  $H/E$  for nanocomposite films varies in the range between 0 and 0.1. The variation in the  $H/E$  values at 1 mN load is shown in Figure S6a. The minimum value of  $H/E$  is 0.0531, obtained for pure PMMA, which is then increased to 0.0541 with the addition of 0.25% of NGP and then shows a remarkable increase of 0.0592 for P-GMA-N1.25. The increase in the value of  $H/E$  exhibits that a higher wear resistance of the P-GMA-NGP composites corresponds to lesser plastic deformation. Thus, P-GMA-NGP composites seem to be more appropriate for hard protective and high wear resistance coating for

aerospace automobile applications. The  $E$  versus  $H$  graph depicts a linear path indicating the toughness of the material.<sup>55</sup> Figure S6b shows the  $E/H$  values deviated from thumb rule, which is expected for a polymer material. However, the parallel trend was observed for P-GMA-NGP composites with respect to the standard rule of thumb which depicts that these nanocomposites exhibit better mechanical properties. Load versus displacement curves are further used to calculate the elastic recovery (ER). Figure S6c depicts the variation elastic recovery for polymer nanocomposite films at various NGP loadings. In comparison with pure PMMA, the P-GMA-N1.25 shows 60.3% of elastic recovery exhibiting highest strength of the composite which restricts the indenter. In addition, the  $h_{res}/h_{max}$  curve of P-GMA-NGPs depicts the opposite trend to that of ER (Figure S6d). The values of this parameter should vary between 0 and 1, where the lower limit corresponds to the rigid plastic behavior. Our result varies between 0.404 and 0.553, which indicates that both elastic and plastic behaviors are present in the P-GMA-NGP composites. To study the elastic and plastic properties in terms of deformation energy, the plastic deformation energy ( $U_r$ ) have also been explored. Generally,  $U_r$  of the polymer composites is estimated by an area surrounded by the loading–unloading curve in the load–displacement profile.<sup>48</sup> In the present case, the values of  $U_r$  are found in the range between  $9.97 \times 10^{-9}$  and  $6.13 \times 10^{-9}$  J as shown in Figure S6e. The value of  $H$  and  $U_r$  are strongly depended upon ER. The results for  $U_r$  are also in good agreement with the results for  $H$ .

It is concluded from the comparison of results in Table 2 that the judicious choice of GMA as the bridging material at the interface region in P-GMA-NGP composites results in the improvement of the nanomechanical properties. Once GMA is introduced in the vicinity of NGP filler, it exhibits the ability to transfer stress from the matrix to the filler. The strongly bound surface layer of PMMA matrix with compatible GMA and NGPs evidently diminishes the interfacial tension between the modified filler and the matrix and suppresses the agglomeration. The synergistic effect of the GMA compatibilizer effectively binds itself across the interface and reduces the interfacial tension between the components and minimizes the dispersed phase coalescence promoting a fine distribution of the NGPs within the PMMA matrix and also reduces the possibility of interfacial failure. The possible mechanism for enhanced nanomechanical properties of P-GMA-NGP (GMA bridging method) over P-NGP/S (solution mixing method) is due to the initial modification of NGP surface by GMA which results in (i) homogeneous dispersion, (ii) large volume of interfaces, (iii) reactive sites, and (iv) strong covalent bonding with PMMA. The as-prepared P-GMA-NGP composite material can withstand the compression, extension breaking, and bending as per the requirement of the aerospace and automobile industry.

The electrical property of the carbon-based polymer composites was closely related to the dispersion state of carbon filler in the matrix. The electrical conductivity of P-GMA-NGP composite was expected to have a lower percolation threshold and a higher conductivity at a lower NGP loading, which not only decreases the cost of the composite but also preserves the processability of the composite system. The ability to transform an insulating polymer into a conductor is strongly desired. The variation in electrical conductivity of P-GMA-NGP composite as a function of NGP wt % is shown in Figure 6a.

The percolation phenomenon explains the method of forming a conducting network using a conducting nanofiller within the insulating host polymer matrices.<sup>37,38</sup> According to the percolation theory, the electrical conductivity of the polymer nanocomposite above the percolation threshold ( $\mu_c$ ) value depends on the weight percentage by scaling law.<sup>56</sup>

$$\sigma = \sigma_0(\mu - \mu_c)t \quad (1)$$

where  $\sigma$  is the electrical conductivity of the polymer nanocomposite,  $\sigma_0$  is the electrical conductivity of the filler,  $\mu$  is the weight percentage of NGPs,  $\mu_c$  is the percolation threshold, and  $t$  is the exponent.

At a percolation threshold ( $\mu_c$ ), the nanofillers construct the interconnected networks of conducting paths throughout the insulating polymer matrix and thus encourage a transition of insulator-to-conductor corresponding to a steep increase in the electrical current of composites. The percolation in the P-GMA-NGP composites was measured to occur at the filler concentration ( $\mu_c$ ) of 0.75 wt %. Above the percolation threshold, the electrical conductivity of composites rapidly rises up to  $\sim 3.2 \times 10^{-1}$  at 1.25 wt %. The inset of the figure depicts the  $\sigma$  versus  $(\mu - \mu_c)$  double logarithmic plot, which evaluates 1.80 conductivity exponent value ( $t$ ). It should be noted that the calculated  $t$  values lying in the range of 1.6–2 indicate the construction of three-dimensional networks.<sup>57</sup> At that particular stage, the tunneling effect occurs between the neighboring platelets of nanographite, which makes the composite a useful multifunctional material (Figure 6b). All of the values of percolation threshold and the electrical conductivity were averaged from four to five different samples.

The temperature-dependent electrical conductivity has been investigated to explore the nature of charge transport and the mechanism of electrical conduction. The standard two probe-method was employed to study the conduction mechanism by using direct current conductivity versus temperature ranging from 300 to 500 K. Figure 6c shows the log conductivity versus  $1000/T$  curve for P-GMA-NGP composite depicting an increase in the conductivity with increase in temperature. Electron transport in composite materials normally involves thermally activated transport through tunneling of charge carriers between the nearest-neighbor particles at close proximity, enabling an overlap of electron wave functions of each particle and at greater separations. The variable range hopping (VRH) provides the conductivity through an optimal network of electron-hopping sites.<sup>58</sup>

The increase in the conductivity is because the conduction by the charge-hopping mechanism of NGPs occurred between the polymeric chains. The Mott's variable range hopping model (VRH) is extensively used to demonstrate the conduction mechanism that deals with electric conductivity as a function of temperature for the disordered system.

The analytical equation for temperature conductivity dependence in the VRH model is described by

$$\sigma = \sigma_0 \exp \left[ - \left( \frac{T_0}{T} \right)^{1/4} \right] \quad (2)$$

where  $\sigma_0$  is the pre-exponential constant and  $T_0$  is the Mott's characteristic temperature, which is calculated by the relationship given in eq 3

$$T_0 = \frac{\lambda}{[K_B n(E_F) \alpha^3]} \quad (3)$$

The localized states ( $T_0$  decreases with the increase in NGP wt % which exhibits a straight line between  $\log \sigma$  versus  $1/T^{-1/4}$ , indicating the relation of conductivity with polaron transport (Figure 6d). Two other important parameters introduced by Mott, the average hopping distance ( $R$ ) between two localized states and the average hopping energy ( $E$ ), were determined by using the following expressions

$$R = \left\{ \frac{9\alpha}{[8\pi K_B T n(E_F)]} \right\}^{1/4} \quad (4)$$

$$E = \frac{3}{4\pi R^3 n(E_F)} \quad (5)$$

P-GMA-NGP composites exhibit a large surface area due to the incorporation of NGP filler in the host PMMA matrix. As the concentration of NGP increases from 0.25 to 1.25 wt % for P-GMA-NGP composite system, both hopping distance and hopping energy decrease. The incorporation of NGP filler within the composite system enhanced the localized states of the charge carrier. Moreover, the increase in temperature causes diffusion of the polymeric chains into the galleries of the nanofillers, which promotes the exfoliation along with the dispersion of NGPs within the composite system. The improved dispersion results in increased  $N(E_F)$  states along with a decrease in hopping distance; hence, a reduced amount of energy is required for the carriers to create a transition between the two different localized states.<sup>58–60</sup> To compare the electrical properties of P-GMA-NGPs, the composites were also prepared by solution-blending method. The enhanced electrical property of P-GMA-NGPs over P-NGP/S was probably due to the strong interfacial interaction between the uniformly dispersed modified NGPs and PMMA matrix, which favors the hopping mechanism. Moreover, the agglomeration of NGPs in P-NGP/S composite is responsible for low conduction. The values obtained from the equations of hopping conduction mechanism for both GMA bridging and solution blending methods are summarized in Table 3.

## CONCLUSIONS

We have successfully demonstrated a novel strategy for the facile synthesis of P-GMA-NGPs nanocomposite, where GMA acts as a bridge between NGPs and PMMA. Further, GMA bridging in P-GMA-NGP nanocomposite exhibits a remarkable

**Table 3. Representation of the Mott's Variable Parameters for P-GMA-NGPs and P-NGP/S as a Function of NGP wt %**

composition	$T_0$ (K)	density of states at Fermi level $N(E_F)$ ( $\text{eV}^{-1} \text{cm}^{-3}$ )	hopping distance	average hopping distance energy (meV)
P-GMA-N0.25	$9.22 \times 10^6$	$2.28 \times 10^{19}$	$4.96 \times 10^{-7}$	856
P-GMA-N0.5	$8.78 \times 10^6$	$2.39 \times 10^{19}$	$4.90 \times 10^{-7}$	846
P-GMA-N0.75	$8.81 \times 10^3$	$2.38 \times 10^{22}$	$8.73 \times 10^{-8}$	150
P-GMA-N1	$7.21 \times 10^3$	$2.91 \times 10^{22}$	$8.30 \times 10^{-8}$	143
P-GMA-N1.25	$5.20 \times 10^4$	$4.04 \times 10^{21}$	$1.36 \times 10^{-7}$	235
P-N0.25/S	$6.40 \times 10^8$	$3.28 \times 10^{19}$	$4.533 \times 10^{-7}$	299
P-N0.5/S	$5.71 \times 10^6$	$3.67 \times 10^{19}$	$4.408 \times 10^{-7}$	267
P-N0.75/S	$4.45 \times 10^6$	$4.72 \times 10^{19}$	$4.139 \times 10^{-7}$	208
P-N1/S	$3.54 \times 10^6$	$5.93 \times 10^{19}$	$3.909 \times 10^{-7}$	165
P-N1.25/S	$2.45 \times 10^6$	$8.57 \times 10^{19}$	$3.566 \times 10^{-7}$	114

enhancement in the mechanical (elastic modulus, hardness, stiffness, hard protective, elastic recovery, wear resistance), thermal (thermal decomposition temperature, glass transition temperature), and electrical properties (conductivity), which are confirmed through nanoindentation, TGA/DSC, and two-probe techniques, respectively. Thus, the exceptional feature of P-GMA-NGP multifunctional nanocomposite provides mechanically strong, flexible, robust, and thermally stable material, which could be potentially used in aerospace applications and automobile industry.

## METHODS

**Materials and Chemicals.** The NGPs were prepared from graphite flakes obtained by Asbury Carbon Inc. Purified MMA monomer (Sigma-Aldrich) was extracted by sodium hydroxide solution. Glycidyl methacrylate (GMA) and 3-aminopropyl trimethoxysilane (APTMS) were supplied from Sigma-Aldrich. All of the other organic solvents used in this study were of analytical grade and were used without further purification.

**P-GMA-NGP Composite Synthesis.** The NGPs were prepared by modified Hummer's method as reported earlier.<sup>20</sup> The 0.5 g of the acid-treated NGPs (A-NGPs) were introduced into 100 ml of ethanol containing 1% APTMS, and the mixture was stirred at 80 °C for 12 h. The APTMS-treated NGPs were again washed with ethanol and then dried under vacuum at room temperature. Finally, the APTMS-NGP was reacted with GMA (compatibilizer) for 8 h at 120 °C within the solution of  $\text{CHCl}_3$ . The functionalized NGPs (GMA-f-NGPs) were dried in vacuum oven for 12 h at 80 °C. Finally, the polymer composite (P-GMA-NGPs) comprising poly(methyl methacrylate) and GMA-functionalized NGP were prepared by in situ polymerization. The GMA-f-NGPs ranging from 0.25 to 1.25 wt % NGP loading were dispersed and sonicated in 10 g of MMA monomer for 1 h and the reaction mixtures of the composites were added in a three-neck round-bottom flask. The reaction flask was stirred at 80 °C for 5 h under  $\text{N}_2$  atmosphere. The polymerization proceeds with the addition of AIBN to the mixture while stirring. The resulting P-GMA-NGPs was filtered and washed repeatedly with methanol and dried for 24 h in a vacuum. The schematic representation depicting the stepwise synthesis of P-GMA-NGP composites is described in Figure S7.

**Characterization. Structural Properties.** Fourier transform infrared (FTIR) spectra were recorded with KBr pellets on Nicolet 5700 FTIR spectrophotometer at a resolution of 4  $\text{cm}^{-1}$ . The scanned wave numbers ranged from 400 to 4000  $\text{cm}^{-1}$ . The X-ray photoelectron spectroscopy (XPS) measurements were conducted on a micron technology XPS (ESCA+) spectrophotometer. The surface morphology of the composite films was analyzed by Zeiss MA EVO-18 Special edition SEM. The high-resolution transmission electron microscope (HRTEM), JEOL 2100F instrument was employed to study the morphology of the polymer nanocomposite films. The sample for HRTEM analysis was prepared by depositing an aliquot of the sample suspension onto a carbon grid and then the solvent was allowed to evaporate. The X-ray diffraction (XRD) studies of the composites were measured by using Rigaku Miniflex. The X-ray diffractometer with  $\text{Cu K}\alpha$  radiation scanned from 5 to 45 °C with an increment of 0.02° every 0.6 s. The average molecular weight of the composite system was determined by gel permeation chromatography (GPC), Turbo matrix-40 with THF as an eluent.

**Thermal Properties.** The DSC was conducted on a Shimadzu DSC 60 instrument using nitrogen flow from room temperature at 400 to 10 °C min<sup>-1</sup>. The thermogravimetric analysis (TGA) was performed with (Mettler Toledo TGA/SDTA851e) a thermogravimetric analyzer under an inert atmosphere (owing N<sub>2</sub> gas) ranging from 25 to 700 °C at a heating rate of 10 °C min<sup>-1</sup>.

**Mechanical Properties.** The mechanical properties of the polymer nanocomposites at varying NGP loadings were measured by using an IBIS nanoindentation system (model B, Fisher Cripps Laboratories Pvt. Ltd., Australia) at room temperature. The maximum load of 500 mN along with force resolution of 500 nN, depth resolution of 0.03 nm, and depth of 20 nm was applied. A Berkovich indenter was used for testing the samples with a face angle of 65.27° and tip radius of 100 nm. All of the samples were collected and analyzed automatically by using the software provided by the manufacturer.

**Electrical Properties.** The conductivity of P-GMA-NGPs was measured by using a standard two-probe technique using a Keithley programmable current source (model 6517B) at room temperature with rectangular (2 cm × 2 cm) films and silver paste ohmic contacts at the edges of the films. The temperature-dependent conductivity measurements were performed by placing the above setup in the oven with a gradual increase in temperature (300–500 K) corresponding to the electrical conductivity of the composites.

## ■ ASSOCIATED CONTENT

### ● Supporting Information

The Supporting Information is available free of charge on the ACS Publications website at DOI: 10.1021/acsomega.8b00194.

Digital images of composite; dispersion of P-GMA-NGP in organic solvents; XRD spectra; 2D patterns of P-GMA-NGP composites; SEM images of the fractured surface; optical microscope images; mechanical properties; conductivity vs inverse of absolute temperature for P-NGP/S composite; schematic illustration of the free standing P-GMA-NGPs composite preparation process (PDF)

## ■ AUTHOR INFORMATION

### Corresponding Authors

\*E-mail: [srattan@amity.edu](mailto:srattan@amity.edu) (S.R.).

\*E-mail: [bipinbhu@yahoo.com](mailto:bipinbhu@yahoo.com) (B.K.G.).

### ORCID

Sunita Rattan: 0000-0001-9396-704X

Bipin Kumar Gupta: 0000-0002-0176-0007

### Author Contributions

The manuscript was written through contributions of all the authors. All of the authors have given approval to the final version of the manuscript.

### Notes

The authors declare no competing financial interest.

## ■ REFERENCES

- (1) Fim, F.; Guterres, J. M.; Basso, N. R. S.; Galland, G. B. Polyethylene/graphite nanocomposites obtained by in situ polymerization. *J. Polym. Sci., Part A: Polym. Chem.* **2010**, *48*, 692.
- (2) Cho, D.; Lee, S.; Yang, G.; Fukushima, H.; Drzal, L. T. Dynamic mechanical and thermal properties of phenylethynl-terminated

polyimide composites reinforced with expanded graphite nanoplatelets. *Macromol. Mater. Eng.* **2005**, *290*, 179–187.

- (3) Kim, S.; Drzal, L. T. Comparison of exfoliated graphite nanoplatelets (xGnP) and CNTs for reinforcement of EVA nanocomposites fabricated by solution compounding method and three screw rotating systems. *J. Adhes. Sci. Technol.* **2009**, *23*, 1623–1638.

- (4) Ramanathan, T.; Abdala, A. A.; Stankovich, S.; Dikin, D. A.; Herrera-Alonso, M.; Piner, R. D.; Adamson, D. H.; Schniepp, H. C.; Chen, X.; Ruoff, R. S.; Nguyen, S. T.; Aksay, I. A.; Prud'Homme, R. K.; Brinson, L. C. Functionalized graphene sheets for polymer nanocomposites. *Nat. Nanotechnol.* **2008**, *3*, 327–331.

- (5) Yu, A.; Ramesh, P.; Itkis, M. E.; Bekyarova, E.; Haddon, R. C. Graphite Nanoplatelet–Epoxy Composite Thermal Interface Materials. *J. Phys. Chem. C.* **2007**, *111*, 7565–7569.

- (6) Veca, L. M.; Meziani, M. J.; Wang, W.; Wang, X.; Lu, F.; Zhang, P.; Lin, Y.; Fee, R.; Connell, J. W.; Sun, Y.-P. Carbon Nanosheets for Polymeric Nanocomposites with High Thermal Conductivity. *Adv. Mater.* **2009**, *21*, 2088–2092.

- (7) Chen, Y.; Tao, J.; Li, S.; Khashab, N. M. Compositing Polyetherimide with Polyfluorene Wrapped Carbon Nanotubes for Enhanced Interfacial Interaction and Conductivity. *ACS Appl. Mater. Interfaces* **2014**, *6*, 9013–9022.

- (8) Wang, G.; Dai, Z.; Liu, L.; Hu, H.; Dai, Q.; Zhang, Z. Tuning the Interfacial Mechanical Behaviors of Monolayer Graphene/PMMA Nanocomposites. *ACS Appl. Mater. Interfaces* **2016**, *8*, 22554–22562.

- (9) Wang, Y.; Yang, C.; Pei, Q. X.; Zhang, Y. Some Aspects on Thermal Transport across the Interface between Graphene and Epoxy in Nanocomposites. *ACS Appl. Mater. Interfaces* **2016**, *8*, 8272–8279.

- (10) Wang, P.; Zhang, J.; Dong, L.; Sun, C.; Zhao, X.; Ruan, Y.; Lu, H. Interlayer Polymerization in Chemically Expanded Graphite for Preparation of Highly Conductive, Mechanically Strong Polymer Composites. *Chem. Mater.* **2017**, *29*, 3412–3422.

- (11) Li, W.; Shang, T.; Yang, W.; Yang, H.; Lin, S.; Jia, X.; Cai, Q.; Yang, X. Effectively Exerting the Reinforcement of Dopamine Reduced Graphene Oxide on Epoxy-Based Composites via Strengthened Interfacial Bonding. *ACS Appl. Mater. Interfaces* **2016**, *8*, 13037–13050.

- (12) Tang, L.-C.; Wan, Y.-J.; Yan, D.; Pei, Y.-B.; Zhao, L.; Li, Y.-B.; Wu, L.-B.; Jiang, J.-X.; Lai, G.-Q. The Effect of Graphene Dispersion on The Mechanical Properties of Graphene/Epoxy Composites. *Carbon* **2013**, *60*, 16–27.

- (13) Xu, D.; Sridhar, V.; Pham, T. T.; Kim, J. K. Dispersion, Mechanical and Thermal Properties of Nano Graphite Platelets Reinforced Fluoroelastomer Composites. *e-Polym.* **2013**, *8*, 237–255.

- (14) Green, P. F. The structure of chain end-grafted nanoparticle/homopolymer nanocomposites. *Soft Matter* **2011**, *7*, 7914–7926.

- (15) Awasthi, A. P.; Lagoudas, D. C.; Hammer, D. C. Modeling of graphene–polymer interfacial mechanical behavior using molecular dynamics. *Modell. Simul. Mater. Sci. Eng.* **2009**, *17*, No. 015002.

- (16) Rudolf, C.; Boesl, B.; Agarwal, A. In situ indentation behavior of bulk multi-layer graphene flakes with respect to orientation. *Carbon* **2015**, *94*, 872–878.

- (17) Lago, E.; Toth, P. S.; Pugliese, G.; Pellegrini, V.; Bonaccorso, F. Solution blending preparation of polycarbonate/graphene composite: boosting the mechanical and electrical properties. *RSC Adv.* **2016**, *6*, 97931–97940.

- (18) Kumar, A.; Bansal, A.; Behera, B.; Jain, S. L.; Ray, S. S. Ternary hybrid polymeric nanocomposites through grafting of polystyrene on graphene oxide-TiO<sub>2</sub> by surface initiated atom transfer radical polymerization (SI-ATRP). *Mater. Chem. Phys.* **2016**, *172*, 189–196.

- (19) Zhang, Y.; Choi, J.; Park, S.-J. Thermal conductivity and thermo-physical properties of nanodiamond-attached exfoliated hexagonal boron nitride/epoxy nanocomposites for microelectronics. *Composites, Part A* **2017**, *101*, 227–236.

- (20) Zhang, Y.; Park, S.-J. In-situ modification of nanodiamonds by mercapto-terminated silane agent for enhancing the mechanical interfacial properties of nitrile butadiene rubber nanocomposites. *Polym. Compos.* **2017**, 1–10.

- (21) Zhang, Y.; Li, X.; Xin Fei, G.; Ur, D.; Cho, R. Effect of coupling agents and ionic liquid on the properties of rice bran carbon/carboxylated styrene butadiene rubber composites. *Macromol. Res.* **2015**, *23*, 952–959.
- (22) Singhal, P.; Rattan, S. Swift Heavy Ion Irradiation as a Tool for Homogeneous Dispersion of Nanographite Platelets within the Polymer Matrices: Towards Tailoring the Properties of PE-DOT:PSS/Nanographite Nanocomposites. *J. Phys. Chem. B* **2016**, *120*, 3403–3413.
- (23) Mazumdar, P.; Rattan, S.; Mukherjee, M. Polymer nanocomposites using click chemistry: novel materials for hydrogen peroxide vapor sensors. *RSC Adv.* **2015**, *5*, 69573–69582.
- (24) Mazumdar, P.; Chockalingam, S.; Rattan, S. Strategy to synthesise nano-engineered polymer nanocomposite with a mechanically strong interface: a highly flexible ammonia gas sensor. *RSC Adv.* **2016**, *6*, 73269–73281.
- (25) Ye, Y.-S.; Chen, Y.-N.; Wang, J.-S.; Rick, J.; Huang, Y.-J.; Chang, F.-C.; Hwang, B.-J. Versatile Grafting Approaches to Functionalizing Individually Dispersed Graphene Nanosheets Using RAFT Polymerization and Click Chemistry. *Chem. Mater.* **2012**, *24*, 2987–2997.
- (26) Kou, L.; He, H.; Gao, C. Click chemistry approach to functionalize two-dimensional macromolecules of graphene oxide nanosheets. *Nano-Micro Lett.* **2010**, *2*, 177–183.
- (27) Shim, Y.-S.; Par, S.-J. Influence of Glycidyl Methacrylate Grafted Multi-walled Carbon Nanotubes on Viscoelastic Behaviors of Polypropylene Nanocomposites. *Carbon Lett.* **2010**, *11*, 311–315.
- (28) Buga, M.-R.; Zaharja, C.; Balan, M.; Bressy, C.; Ziarelli, F.; Margaillan, A. Surface modification of silk fibroin fibers with poly(methyl methacrylate) and poly(tributylsilyl methacrylate) via RAFT polymerization for marine antifouling applications. *Mater. Sci. Eng., C* **2015**, *51*, 233–241.
- (29) Sun, G.; Li, X.; Qu, Y.; Wang, X.; Yan, H.; Zhang, Y. Preparation and Characterization of Graphite Nanosheets from Detonation Technique. *Mater. Lett.* **2008**, *62*, 703–706.
- (30) Matsumoto, M.; Saito, Y.; Park, C.; Fukushima, T.; Aida, T. Ultrahigh-throughput Exfoliation of Graphite into Pristine ‘Single-layer’ Graphene using Microwaves and Molecularly Engineered Ionic Liquids. *Nat. Chem.* **2015**, *7*, 730–736.
- (31) Chen, X.; Meng, F.; Zhou, Z.; Tian, X.; Shan, L.; Zhu, S.; Xu, X.; Jiang, M.; Wang, L.; Hui, D.; Wang, Y.; Lu, J.; Gou, J. One-step synthesis of graphene/polyaniline hybrids by in situ intercalation polymerization and their electromagnetic properties. *Nanoscale* **2014**, *6*, 8140–8148.
- (32) Wang, L.; Zhang, L.; Tian, M. Improved polyvinylpyrrolidone (PVP)/graphite nanocomposites by solution compounding and spray drying. *Polym. Adv. Technol.* **2012**, *23*, 652–659.
- (33) Tseng, I.-H.; Chang, J.-C.; Huang, S.-L.; Tsai, M.-H. Enhanced thermal conductivity and dimensional stability of flexible polyimide nanocomposite film by addition of functionalized graphene oxide. *Polym. Int.* **2013**, *62*, 827–835.
- (34) Xu, L.; Fang, Z.; Song, P.; Peng, M. Surface-initiated graft polymerization on multiwalled carbon nanotubes pretreated by corona discharge at atmospheric pressure. *Nanoscale* **2010**, *2*, 389–393.
- (35) Yu, Y.-H.; Lin, Y.-Y.; Lin, C.-H.; Chan, C.-C.; Huang, Y.-C. High performance polystyrene/graphene-based nanocomposites with excellent anti-corrosion properties. *Polym. Chem.* **2014**, *5*, 535–550.
- (36) Kumar, P.; Yu, S.; Shahzad, F.; Hong, S. M.; Kim, Y.-H.; Koo, C. M. Ultrahigh Electrically and Thermally Conductive Self-Aligned Graphene/Polymer Composites Using Large-Area Reduced Graphene Oxides. *Carbon* **2016**, *101*, 120–128.
- (37) Salavagione, H. J.; Quiles-Díaz, S.; Enrique-Jimenez, P.; Martínez, G.; Ania, F.; Flores, A.; Gómez-Fatou, M. A. Development of Advanced Elastomeric Conductive Nanocomposites by Selective Chemical Affinity of Modified Graphene. *Macromolecules* **2016**, *49*, 4948–4956.
- (38) Asgari, M.; Masoomi, M. Thermal and impact study of PP/PET fibre composites compatibilized with Glycidyl Methacrylate and Maleic Anhydride. *Composites, Part B* **2012**, *43*, 1164–1170.
- (39) Kim, K.-S.; Byun, J.-H.; Lee, G.-H.; Park, S.-J. Influence of GMA Grafted MWNTs on Physical and Rheological Properties of PMMA-based Nanocomposites by in situ Polymerization. *Macromol. Res.* **2011**, *19*, 14–20.
- (40) Ou, B.; Zhou, Z.; Liu, Q.; Liao, B.; Yi, S.; Ou, Y.; Zhang, X.; Li, D. Covalent functionalization of graphene with poly(methyl methacrylate) by atom transfer radical polymerization at room temperature. *Polym. Chem.* **2012**, *3*, 2768–2775.
- (41) Gan, L.; Shang, S.; Yuen, C.; Jiang, S. Covalently functionalized graphene with D-glucose and its reinforcement to poly(vinyl alcohol) and poly(methyl methacrylate). *RSC Adv.* **2015**, *5*, 15954–15961.
- (42) Fox, T. G.; Flory, P. J. The glass temperature and related properties of polystyrene. Influence of molecular weight. *J. Polym. Sci.* **1954**, *14*, 315–319.
- (43) Díez-Pascual, A. M.; Gómez-Fatou, M. A.; Ania, F.; Flores, A. Nanoindentation in polymer nanocomposites. *Prog. Mater. Sci.* **2015**, *67*, 1–94.
- (44) Khan, M. K.; Fitzpatrick, M. E.; Hainsworth, S. V.; Edwards, L. Effect of residual stress on the nanoindentation response of aerospace aluminium alloys. *Comput. Mater. Sci.* **2011**, *50*, 2967–2976.
- (45) Hay, J. L.; Pharr, G. M. *Instrumented Indentation Testing*. ASM Handbook; ASM International: Materials Park, OH, 2000; Vol. 8, pp 232–243.
- (46) Lee, S.-H.; Wang, S.; Pharr, G. M.; Xu, H. Evaluation of interphase properties in a cellulose fiber-reinforced polypropylene composite by nanoindentation and finite element analysis. *Composites, Part A* **2007**, 1517–1524.
- (47) Yan, W.; Lun Pun, C.; Wua, Z.; Simon, G. P. Some issues on nanoindentation method to measure the elastic modulus of particles in composites. *Composites, Part B* **2011**, *42*, 2093–2097.
- (48) Oliver, W. C.; Pharr, G. M. An improved technique for determining hardness and elastic modulus using load and displacement sensing indentation experiment. *J. Mater. Res.* **1992**, *7*, 1564–1583.
- (49) Li, X.-F.; Lau, K.-T.; Yin, Y.-S. Mechanical properties of epoxy-based composites using coiled carbon nanotubes. *Compos. Sci. Technol.* **2008**, *68*, 2876–2881.
- (50) Shokrieh, M. M.; Hosseinkhani, M. R.; Naimi-Jamal, M. R.; Tourani, H. Nanoindentation and nanoscratch investigations on graphene-based nanocomposites. *Polym. Test.* **2013**, *32*, 45–51.
- (51) Poon, B.; Rittel, D.; Ravichandran, G. An analysis of nanoindentation in linearly elastic solids. *Int. J. Solids Struct.* **2008**, *45*, 6018–6033.
- (52) Gupta, T. K.; Singh, B. P.; Dhakate, S. R.; Singh, V. N.; Mathur, R. B. Improved nanoindentation and microwave shielding properties of modified MWCNT reinforced polyurethane composites. *J. Mater. Chem. A* **2013**, *1*, 9138–9149.
- (53) Yang, Y.; He, C.-E.; Tang, W.; Tsui, C. P.; Shi, D.; Sun, Z.; Jian, T.; Xie, X. Judicious selection of bifunctional molecules to chemically modify graphene for improving nanomechanical and thermal properties of polymer composites. *J. Mater. Chem. A* **2014**, *2*, 20038–20047.
- (54) Moura, F.; Simões, A. Z.; Paskocimas, C. A.; Zaghet, M. A.; Varela, J. A.; Longo, E. Temperature dependence on the electrical properties of Ba(Ti<sub>0.90</sub>Zr<sub>0.10</sub>)O<sub>3</sub>-2V ceramics. *Mater. Chem. Phys.* **2010**, *123*, 772–775.
- (55) Charitidis, C. A. Nanomechanical and nanotribological properties of carbon-based thin films: A review. *Int. J. Refract. Met. Hard Mater.* **2010**, *28*, 51–70.
- (56) Stauffer, D.; Aharony, A. *Introduction to Percolation, Theory*; Taylor and Francis: London, 1994.
- (57) Gao, J. F.; Li, Z. M.; Meng, Q. J.; Yang, Q. *Mater. Lett.* **2008**, *62*, 3530–3532.
- (58) Nandi, D.; Maity, A. Synthesis, Nanostructure Evaluation and Tunable Anomalous 3D Hopping Transport of Manganese Ferrite Encapsulated Poly[3,4-(Ethyleneoxy)Thiophene Decorated Graphene Layer. *RSC Adv.* **2015**, *5*, 36149.
- (59) Park, W.; Hu, J.; Jauregui, L. A.; Ruan, X.; Chen, Y. P. Electrical and thermal conductivities of reduced graphene oxide/polystyrene composites. *Appl. Phys. Lett.* **2014**, *104*, No. 113101.

(60) Hasnaoui, M. E. L.; Abazine, K.; Achour, M. E.; Costa, L. C. Mott-hopping processes in polymethylmethacrylate matrices filled with polypyrrole particles. *J. Optoelectron. Adv. Mater.* **2016**, *18*, 389–393.